


pH-Responsive Hyaluronic Acid Nanoparticles for Enhanced Triple Negative Breast Cancer Therapy

Xiangle Zeng*, Hairong Wang*, Yawen Zhang , Xue Xu, Xinyi Yuan, Jianchun Li

School of Pharmacy, Bengbu Medical College, Bengbu, 233030, People's Republic of China

*These authors contributed equally to this work

Correspondence: Jianchun Li, School of Pharmacy, Bengbu Medical College, Bengbu, 233030, People's Republic of China, Tel +86 552-3175066, Email Lijc66577@sohu.com

Purpose: This study emphasized that dasatinib (DAS) and olaparib (OLA) have synergistic effects on triple negative breast cancer, by inducing DNA damage and inhibiting DNA damage repair. However, poor water solubility, short half-life of drugs, and low drug concentration in tumor tissue limit the clinical application.

Methods: In this research, acid-sensitive ester bonds were used to connect hydrophobic DAS and hydrophilic hyaluronic acid (HA) to form the amphiphilic polymer prodrug HA-DAS, and then OLA was added as the core, the HA-DAS was used as the carrier to form nanomicelles (HDO-NPs) in aqueous. The characterization and drug release of HDO-NPs were studied, and the cytotoxicity, targeting effect, and intracellular transport behavior of HDO-NPs were evaluated in MDA-MB-231. In addition, the pharmacokinetic and therapeutic effect of HDO-NPs were further verified in vivo.

Results: In vitro characterizations showed that HDO-NPs were spherical with uniform particle size, good stability and anti-dilution ability, and displayed favorable pH-responsive drug release behavior. In addition, the cell experiments showed that HDO-NPs could be effectively taken up by binding to the overexpressed CD44 proteins of MDA-MB-231 cells, resulting in increased intracellular drug concentration. In vivo experiments showed that HDO-NPs can effectively target tumor tissues, have excellent therapeutic effects on tumor, significantly prolong the circulation time of drugs in vivo, and effectively improved the bioavailability of drugs.

Conclusion: DAS and OLA were designed into micelles, the efficacy of HDO-NPs was higher than that of free drugs. Therefore, HDO-NPs have good application prospects in the treatment of triple negative breast cancer.

Keywords: hyaluronic acid, dasatinib, olaparib, combination therapy, polymeric prodrug micelles

Introduction

Design and synthesis of efficient drug delivery systems are crucial for disease treatment and medical development. Polymeric micelle systems have provided a promising strategy.¹⁻³ It is a new nano-preparation obtained by loading small molecule drugs with amphiphilic polymers as carriers, in which the carrier surface can also modify new targeting groups according to the characteristic functional groups to enhance the positioning and recognition function of the system.^{4,5} Meanwhile, the drug encapsulated in the carrier can overcome the defects of short half-life, poor water solubility, poor stability and high side effects of the original drug.⁶⁻¹⁰ Prodrug referred to a class of compounds that have no activity or low activity in vitro and can be transformed by enzyme or non-enzyme to release the active drug after entering the body. After the drug is made into a prodrug, its physical and chemical properties can be improved in many ways, such as increasing water solubility and reducing toxicity.^{11,12} In addition, by introducing stimuli-responsive chemical bonds, prodrugs can have special responses to certain tissues (eg: tumor tissues).¹³⁻¹⁵ Therefore, combined with the advantages of polymeric micelles and prodrug strategies, polymeric prodrug micellar-based drug delivery systems (PPM-DDS) have been widely explored to overcome the shortcomings of conventional chemotherapy and improve antitumor efficacy.^{16,17}

PPM-DDS can improve the efficiency of tumor targeting by enhancing the permeability and retention effect (EPR), thereby improving the bioavailability and therapeutic effect of anti-cancer drugs.¹⁸ Nevertheless, the efficiency of EPR is

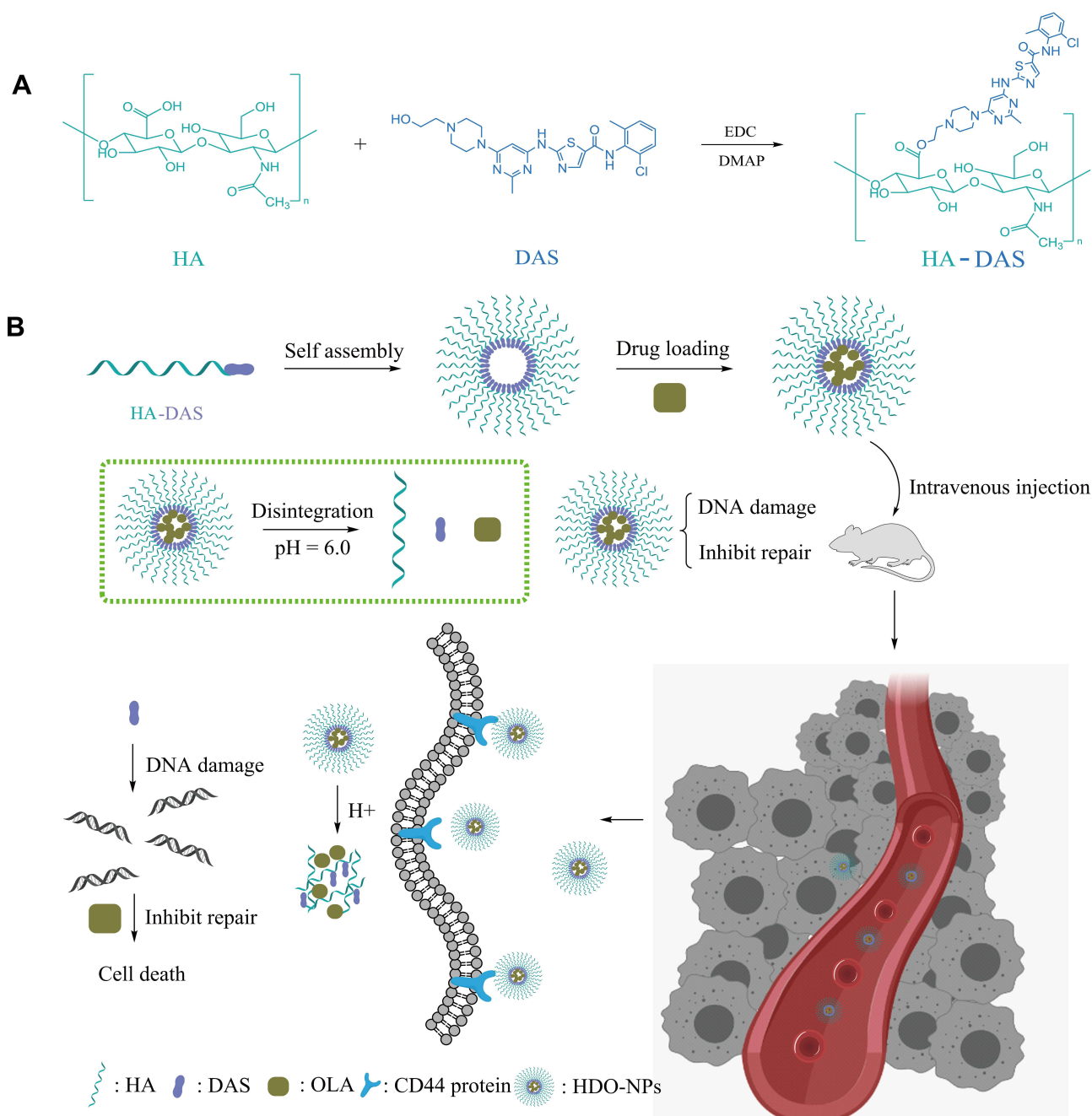
limited by many factors (such as the degree of tumor angiogenesis), poor uptake of tumor cells and incomplete drug release are still problems to be solved. To improve the therapeutic effect of PPM-DDS, researchers have made great efforts to develop drug delivery systems that actively target tumors. Due to the heterogeneity of tumor cells, the expression of some proteins or receptors on the surface is higher than that of normal cells. The CD44 protein has been confirmed to be overexpressed on the surface of various tumor cells, and hyaluronic acid (HA) as its specific ligand has been widely used in targeted drug delivery systems.^{19,20} On the one hand, as a major component of the human intracellular stroma and extracellular matrix, HA has good water solubility and biocompatibility. On the other hand, there are carboxyl and hydroxyl groups in the HA polymer chain, and the chemical reactions around hyaluronic acid include esterification, crosslinking, grafting, amidation and ring-opening reaction on the carboxyl group, which provides a guarantee for the design of the prodrug.²¹ Therefore, PPM-DDS designed and synthesized based on HA can effectively improve the problem of poor uptake of micelles by tumor cells.^{4,22,23}

Owing to the hypoxia and high metabolism of tumor tissue, a large amount of lactic acid accumulation creates acidic internal environment characteristics of tumor tissue. Consequently, PPM-DDS with pH-responsive drug release characteristics are a powerful strategy to achieve selective drug release in tumor cells.^{24–26} At present, various pH-responsive copolymers, including acid-sensitive groups such as ester bonds, hydrazone bonds, and vinyl ethers, have been extensively studied to construct delivery systems for tumor therapy.^{27,28} Taking into account the structure of HA, the ester bond was selected as the connection bond of PPM-DDS, which can effectively improve the problem of incomplete drug release.

In recent years, molecular-targeting drugs for cancer have developed rapidly and a considerable number of blockbuster drugs have been marketed. They can reconstruct normal molecules and inhibit the production of defective molecules, as well as inhibit tumor growth by targeting specific phenotypes of tumor cells.²⁹ However, the growth rate of tumor cells does not remain constant due to the tumour tissue progresses from an initial small number of cells to a lethal tumour load, so a single type of drug therapy often has limited benefits. Correspondingly, combined chemotherapy is superior to monotherapy in terms of the objective effective rate and prolonged survival of patients.⁶

Dasatinib (DAS) is a molecular targeted drug targeting tyrosine kinases that has antitumor effects by specifically targeting Src, BCR-ABL and C-kit cytokines.^{30,31} Furthermore, the structure contains a primary alcohol group that can be used for further chemical reactions (such as esterification reactions). Olaparib (OLA) is a poly ADP-ribose polymerase (PARP) inhibitor, which can prevent PARP release from damaged DNA, thereby inhibiting DNA damage repair and causing tumor cell apoptosis.^{32,33} In a previous study, the combined use of Src inhibitors (DAS) and PARP inhibitors (OLA) increased the sensitivity of prostate cancer to OLA, and the inhibition of Src signaling by DAS increased DNA damage in prostate cancer cells, showing favorable therapeutic effects.³⁴ Moreover, in another study, DAS inhibited cell cycle detection point kinase 1 (Chk1) and induced DNA damage, while OLA inhibited damaged DNA repair.³⁵ Therefore, the combination of DAS and OLA appears to be a promising treatment for triple negative breast cancer. However, there are many problems in practical applications, such as poor solubility, short half-life, low bioavailability and high risk of adverse reactions, which seriously limit their clinical application.³⁶

To address the above problems, we report a PPM-DDS with active targeting capability. The system takes HA as hydrophilic shell and gives it the characteristics of targeting the CD44 protein. HA was connected with DAS through pH-sensitive ester bonds to form the polymer prodrug HA-DAS (Scheme 1A). Subsequently, HA-DAS was used as the carrier, and OLA was used as the core to self-assemble into polymeric prodrug micelles. The micelles have the following advantages: (i) The hydrophilic HA shell and negative surface charge of micelles prolong their cycle time and reduce non-specific clearance of reticuloendothelial system (RES), (ii) When micelles reach the tumor site, HA specifically binds to the overexpressed CD44 protein on the surface of tumor cells and increases uptake by tumor cells, (iii) Meanwhile, the slightly acidic environment of tumor can destroy the ester bond between HA-DAS, leading to the decomposition of micelles and drug release, (iv) The released DAS and OLA can produce the above synergistic effect, promoting DNA damage and aggravating tumor cell apoptosis (Scheme 1B).



Scheme 1 (A) Synthesis route of the pH-responsive prodrug copolymer HA-DAS. (B) Illustration of the HDO-NPs system for tumor therapy in vivo.

Materials and Methods

Materials

HA was purchased from Huaxi Biotechnology Co. Ltd. (Jinan, China, MW: 8814 Da), DAS and OLA were provided by Macklin Co. Ltd. (Shanghai, China), EDCI and DMAP were purchased from Aladdin Co. Ltd. (Shanghai, China). Dimethyl sulfoxide (DMSO), glacial acetic acid and ammonium acetate were obtained from Macklin Co. Ltd. (Shanghai, China), Lyso-tracker Red was purchased from Beyotime Biotechnology Co. Ltd. (Shanghai, China). HA-DAS polymer was prepared by our research group. Reagents such as methanol and acetonitrile were chromatographic grade and supplied by TEDIA (Ohio, USA).

Animals and Cell Culture

The human breast cancer cell line MDA-MB-231 was cultured in RPMI-1640 complete medium containing 10% fetal bovine serum and 1% penicillin-streptomycin. All cells were cultured in a 37°C cell incubator maintained at 5% CO₂ concentration and 95% relative humidity. The cells could be used for subsequent experiments after entering the logarithmic growth phase. In this study, animals were raised according to animal ethical standards. The 4–5-week-old female BALB/c nude mice were purchased from Hunan Sja Laboratory Animal Co. Ltd. The animal experimental procedure was approved by The Animal Health Committee of Bengbu Medical College on June 25, 2021 (Licence No. 2021143), which met the requirements of the Animal Ethical Standards and Use Committee of Bengbu Medical College.

Acid Dissociation of HA-DAS Polymer

HA-DAS polymer was synthesized by our research group and the structure was confirmed by ¹H-NMR.³⁷ In short, EDCI and DMAP were used to activate the carboxyl group of HA in deionized water, and then DAS was added to form the HA-DAS polymer by ester bond.

Subsequently, the dissociation of DAS from the HA-DAS polymer was investigated under acidic conditions. A certain amount of HA-DAS polymer was dissolved in the release solution (pH 6.0, methanol/water = 1:1, v/v), and 500 µL of the release solution was taken at the preset time (0, 4, 8, 12, 24, 48 h). Then, 500 µL of methanol was added, mixed evenly and centrifuged (5000 rpm, 10 min). The supernatant was taken for HPLC detection.

Preparation and Characterization of HA-DAS/OLA (HDO-NPs)

HDO-NPs were prepared by film dispersion method. In brief, 20 mg HA-DAS polymer was dissolved in 8 mL methanol/water (1:1, v/v) mixed solvent, and then 1 mL OLA (2 mg/mL) solution was added. The mixed solution was obtained by ultrasonic dispersion for 0.5 h in an ice bath. The solvent was removed by a rotary evaporator and the film was dissolved with an appropriate amount of water. The free OLA was filtered through 0.22 µm membrane to obtain HDO-NPs solution. The particle size, PDI and zeta potential of HDO-NPs were measured by Malvern particle size analyzer, and the morphology of HDO-NPs were observed by the transmission electron microscopy (TEM).

Evaluation of Drug Loading and Encapsulation Efficiency

HDO-NPs were hydrolyzed by strong alkaline hydrolysis to determine the drug loading and encapsulation efficiency of DAS and OLA.^{37,38} In short, 4 mg HDO-NPs were dissolved in 1 mL deionized water, 100 µL NaOH (1 mol/L) was added for 0.5 h, and then 100 µL HCl (1 mol/L) was added for neutralization. Subsequently, 3 mL methanol was added to dissolve the cracked DAS and OLA, which were mixed evenly and centrifuged (5000 rpm, 10 min). The supernatant was taken for HPLC detection. The drug loading (DL) and encapsulation efficiency (EE) were calculated according to Formulas 1 and 2.

$$DL\% = \frac{W_1}{W_0} \times 100\% \quad (1)$$

$$EE\% = \frac{W_1}{W_2} \times 100\% \quad (2)$$

W₀: Weight of micelles

W₁: Weight of drug in micelles

W₂: Weight of added drug.

Characterization of the Stability of HDO-NPs

HDO-NPs were dissolved in PBS solutions (pH 6.0, 7.4) and sampled at different time points. The particle size and PDI were determined by Malvern particle size analyzer to investigate the stability of nanoparticles under physiological conditions and tumor microenvironment. Meanwhile, to verify the anti-dilution ability of nanoparticles, HDO-NPs

solution was diluted to different concentrations (2000, 1000, 500, 250, 125, 62.5, 31.25, 15.62, 7.81, 3.91 $\mu\text{g/mL}$) and the particle size and PDI were measured to reflect the dilution stability.

In vitro Drug Release

In vitro drug release performance was determined by the dialysis method. In brief, 4 mL HDO-NPs solution (1 mg/mL) was added into the dialysis bag (MWCO 3500 Da), and then placed in PBS with different pH (7.4, 6.0, 4.0) containing 1% (w/v) Tween-80. At different time intervals (0, 0.5, 1, 2, 4, 8, 12, 24, 36, 48 h), 1 mL dialysis medium was taken, and equal volume of release medium was added. The release solution was filtered through 0.22 μm microporous membrane. HPLC was used to determine the concentration of DAS and OLA and calculate the release degree.

The Cell Uptake of HDO-NPs

The fluorescent dye coumarin 6 (C6) was loaded into HA-DAS to prepare HA-DAS/C6 solution by the film dispersion method. MDA-MB-231 cells were inoculated overnight in 24-well plates at a density of 1×10^4 cells/well and divided into three groups, which were supplemented with fresh medium containing C6 and HA-DAS/C6. Additionally, the other group was preincubated with HA (10 mg/mL) for 0.5 h and then added to medium containing HA-DAS/C6. The cells were cultured at 37°C for 1 h and 4 h, respectively, and washed with PBS solution three times. The samples were fixed with paraformaldehyde for 10 min, stained with DAPI at room temperature for 10 min, and then observed under a fluorescence microscope.

DAS and OLA Accumulation Assay

MDA-MB-231 cells were seeded in 24-well plates (2×10^4 cells/well), then incubated with DAS + OLA, and HDO-NPs (the concentration of DAS was 10 μM) at 37°C for 1, 2 and 4 h. Meantime, the HA preincubation treatment group was set up. After incubation, the supernatant was discarded by centrifugation (2500 rpm, 10 min), and 10 μL cell lysate was added to ice bath for 0.5 h. Next, 2 μL supernatant was centrifuged at 4°C (5000 rpm, 0.5 h) to determine the protein content. Finally, 100 μL methanol was used for ultrasonic extraction of drugs. DAS and OLA concentrations were determined by HPLC, and the drug concentration per unit protein was calculated.

The Intracellular Transport Behavior of HDO-NPs

MDA-MB-231 cells were seeded in a 6-well plate at a density of 5×10^4 cells/well, and cultured in 2 mL fresh medium containing HA-DAS/C6 for 1 and 4 h, respectively. After incubation, 2 mL Lyso-Tracker Red (diluted with 1640 medium) lysosomal staining solution was added to each well, stained at 37°C for 45 min and washed with PBS solution to remove the residual dye. Subsequently, the cells were fixed with paraformaldehyde in the dark for 15 min. Finally, 1 mL DAPI was added to each well for staining at room temperature for 10 min and observed under the fluorescence microscope.

In vitro Cytotoxicity

The toxicity of HDO-NPs to MDA-MB-231 cells was investigated by MTT assay. In brief, MDA-MB-231 cells were seeded in 96-well plates (1×10^4 cells/well) for 24 h. The medium solutions of DAS, OLA, DAS + OLA, and HDO-NPs with a series of concentrations (5, 10, 20, 50, 75, and 100 μM) were prepared, and the old medium was replaced. After incubation for 24 and 48 h, 20 μL MTT solution was added to each well and cultured for 4 h. The absorbance at 490 nm was measured, and the cell survival rate was calculated according to Equation 3.

$$\text{Cell viability}(\%) = \frac{OD1 - OD0}{OD2 - OD0} \times 100\% \quad (3)$$

OD0: Absorbance at 490 nm in blank group

OD1: Absorbance at 490 nm in the drug groups

OD2: Absorbance at 490 nm in the control group.

Calcein-AM/PI Staining

MDA-MB-231 cells were inoculated in 96-well plates at a density of 1×10^4 cells/well for overnight culture, then the medium containing DAS, OLA, DAS + OLA and HDO-NPs (DAS concentration 10 μ M) was added, respectively, and incubated for 24 h. After incubation, calcein-AM/PI double dyeing solution was added and dyed at 37°C for 30 min. Subsequently, the cells were observed under the fluorescence microscope.

Hemolysis Test

Because the administration method of HDO-NPs was intravenous injection, the effect on erythrocytes was investigated. In short, the blood was centrifuged at 2000 rpm at 4°C for 10 min to collect red blood cell suspensions and diluted with PBS solution to 2% (v/v). Subsequently, 100 μ L erythrocyte suspension was mixed with 100 μ L HDO-NPs (5, 10, 20, 50, 75, and 100 μ g/mL). After incubation at 37°C for 2 h, the supernatant was centrifuged (5000 rpm) for 5 min. The absorbance of the supernatant was determined at 570 nm. Deionized water was used as the positive control and PBS solution as the negative control, and the relative hemolysis rate (RHR%) was calculated according to Formula 4.

$$RHR\% = \frac{A_1 - A_0}{A_2 - A_0} \times 100\% \quad (4)$$

A_0 : Absorbance of the PBS treatment group at 570 nm

A_1 : Absorbance of sample group at 570 nm

A_2 : Absorbance of the deionized water treatment group at 570 nm

In vivo Distribution

After the tumor-bearing mice model was successfully established, the Cy5 was encapsulated into HA-DAS by the film dispersion method. Free Cy5 and HA-DAS/Cy5 nanomicelles (Cy5 dose of 10 μ g/mouse) were injected into BALB/c tumor-bearing mice by tail intravenous injection. Subsequently, the mice were anesthetized with isoflurane at 1, 4, 8, 12 and 24 h, respectively. The mice were placed in the small animal living imager for fluorescence scanning and photographing.

In vivo Antitumor Efficacy

MDA-MB-231 tumor-bearing mice were established, and all mice were randomly divided into 5 groups (PBS group, DAS group, OLA group, DAS + OLA group, and HDO-NPs group, $n = 6$) when the subcutaneous tumor was approximately 100 mm³. On day 0, the drug was injected into the tumor-bearing mice, once every 3 days at a concentration of 5 mg/kg. The tumor length and width were measured by vernier caliper before each administration, and tumor volume (V) was calculated according to Equation 5.

$$V = \frac{a \times b^2}{2} \quad (5)$$

a: Tumor length b: Tumor width

After 6 times of administration, the subcutaneous tumors were stripped and photographed. Then, the tumor tissues were stained with HE, Ki67 and γ -H2AX immunofluorescence.

In vivo Safety of HDO-NPs

After treatment, the main organs (heart, liver, spleen, lung and kidney) of mice were taken for HE staining to evaluate the acute toxicity. At the same time, blood was collected for the detection of aspartate aminotransferase (AST), alanine aminotransferase (ALT), alkaline phosphatase (AKP), creatinine (CRE) and other indicators to reflect the in vivo safety of nanoparticles.

Pharmacokinetics

Healthy female SD rats were randomly divided into two groups ($n = 6$) and were injected with (i) free DAS + OLA and (ii) HDO-NPs at a 5 mg/kg DAS-equivalent dose by tail vein injection. Then, 0.5 mL blood sample was removed at

a predetermined time interval and centrifuged at 5000 rpm for 10 min to obtain drug-containing plasma. Afterwards, methanol (300 μ L) was used as the protein precipitator, and diclofenac sodium as internal standard (10 μ L) was added to 90 μ L plasma. The sample was centrifuged at 5000 rpm for 10 min. The plasma concentrations of the two drugs were determined by HPLC, and pharmacokinetic parameters were analyzed by WinNonlin 8.2 software.

Statistical Analysis

All experimental values were expressed as the mean \pm SD, $n = 3$ or 6. Statistical significance (* $p < 0.05$, ** $p < 0.01$, *** $p < 0.001$) was performed by one-way analysis of variance (ANOVA) and nonparametric tests using SPSS.

Results and Discussion

pH-Responsive Hydrolysis of HA-DAS

The amphiphilic polymer HA-DAS was prepared and confirmed by our research group. We aimed to connect HA with DAS by pH-sensitive ester bonds, and the pH-responsive mechanism is shown in Figure 1A. Under the attack of hydrogen ions, the ester bond of HA-DAS breaks to release DAS.³⁹ To verify this mechanism, HPLC was used for detection. As shown in Figure 1B, the retention time of DAS was 4.6 min and that of HA-DAS was 7.2 min. The increase of retention time was caused by the introduction of HA with higher polarity. Moreover, with prolonged incubation time, the peak DAS increased, while the peak HA-DAS decreased and the dissociation rate was approximately 70% at 48 h, indicating that DAS gradually dissociated from HA-DAS. Hence, HA-DAS has good pH responsiveness.

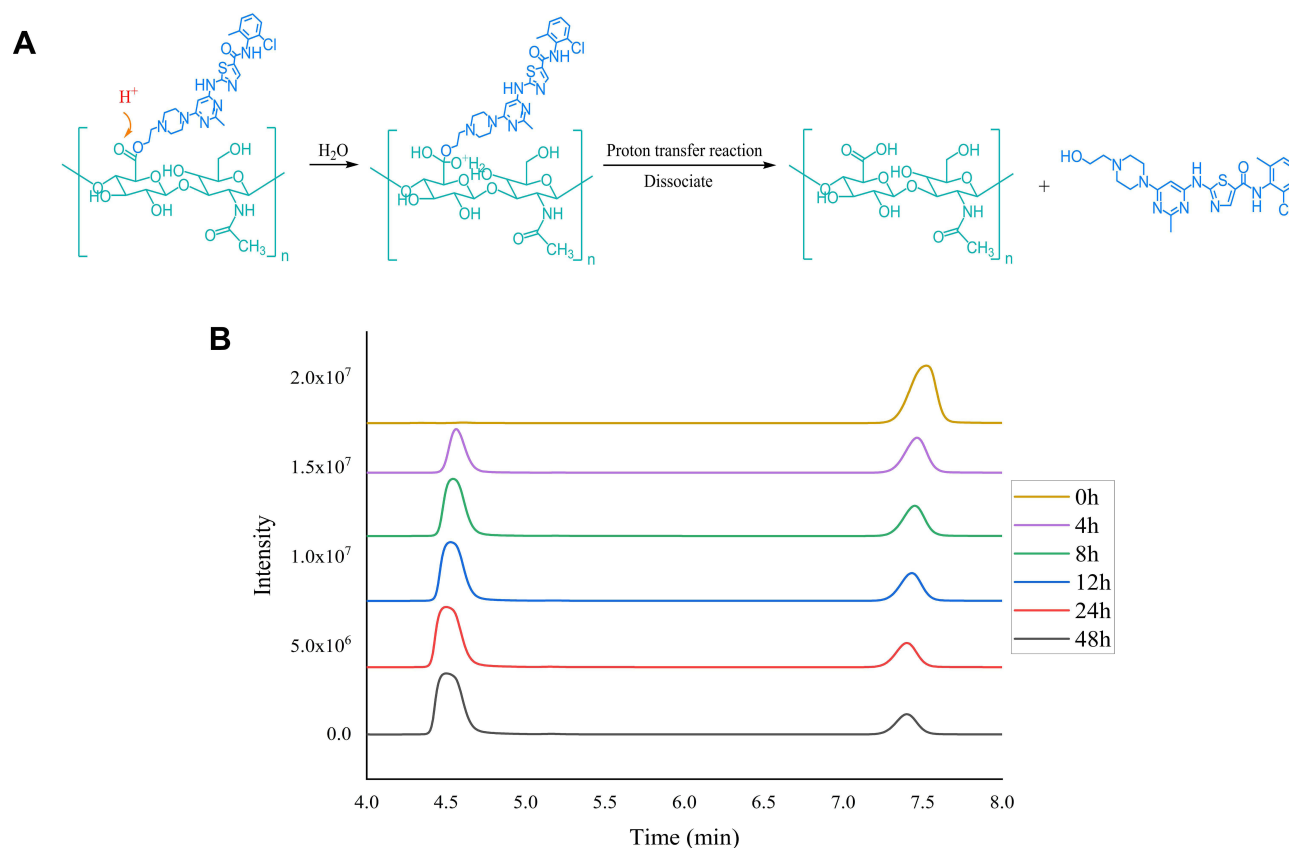


Figure 1 (A) Acid hydrolysis mechanism of HA-DAS. (B) Acid-triggered dissociation of DAS from HA-DAS was detected by HPLC.
Abbreviations: HA, hyaluronic acid; DAS: dasatinib.

Preparation and Characterization of HDO-NPs

HDO-NPs were successfully prepared by the film dispersion method. The particle size, PDI, zeta potential, drug loading and encapsulation efficiency of HDO-NPs were determined. The DL of DAS was $1.68\% \pm 0.29\%$, and the DL and EE of OLA were $7.38\% \pm 0.17\%$ and $84.95\% \pm 1.17\%$, respectively (Table 1), with good reproducibility. Furthermore, Figure 2A and Table 1 show that HDO-NPs had a good hydrodynamic diameter,⁴⁰ the particle size of micelles was (56.18 ± 1.29) nm, and the PDI was 0.23 ± 0.02 . The zeta potential of HDO-NPs was (-7.42 ± 1.22) mV (Table 1). The morphology and dispersion of drug-loaded micelles HDO-NPs were characterized by TEM. The results are shown in Figure 2B, HDO-NPs were spherical, with uniform internal distribution and good dispersion.

Characterization of the Stability of HDO-NPs

The stability of nanoparticles is an important basis for measuring their efficacy. When the nanoparticles are dissolved, the drugs contained in them may be released slowly. Therefore, the stability was evaluated by measuring the particle size and PDI of HDO-NPs. We stored HDO-NPs in PBS solutions (pH 7.4, 6.0) for one week to simulate their stability in normal physiological and tumor microenvironments. As shown in Figure 3A and B, the particle size and PDI of HDO-NPs did not change significantly at pH 7.4, particle size was stabilized at about 55 nm and PDI 0.2, respectively. The results indicated that HDO-NPs have strong stability under physiological conditions, which provided a good basis for their efficacy at the cellular level and in vivo. In contrast, the particle size of HDO-NPs gradually decreased in the slightly acidic environment (pH 6.0), indicating that HDO-NPs were unstable under this condition and gradually disintegrated. The change of PDI also proved this phenomenon, due to the disintegration of nanoparticles, the dispersion of PDI increased.⁴¹

In addition, nanoparticles will be diluted after entering the blood, so HDO-NPs should have anti-dilution ability. In Figure 3C and D, when HDO-NPs were diluted to $3.91 \mu\text{g/mL}$, the particle size and PDI changed little, certifying that HDO-NPs have good anti-dilution ability and can be used for intravenous administration.¹

In vitro Drug Release

The release behavior of HDO-NPs within 48 h at pH 7.4, pH 6.0 and pH 4.0 was measured by the dialysis method, and the cumulative release percentage was calculated. The pH 7.4, pH 6.0 and pH 4.0 conditions were used to simulate the normal physiological environment, slightly acidic tumor environment and intracellular lysosome environment, respectively. As shown in Figure 4A and B, the cumulative release rates of DAS and OLA at pH 7.4 were about 30% and 41%, respectively. In contrast, when the pH values decreased to 6.0 and 4.0, the release rates of DAS and OLA increased significantly. The release of DAS after 48 h of incubation was approximately 56.38% (pH 6.0) and 66.69% (pH 4.0), and that of OLA after 48 h of incubation was about 63.78% (pH 6.0) and 76.58% (pH 4.0). The results showed that HDO-NPs could release more DAS and OLA under slightly acidic conditions. Additionally, the cumulative release rate of DAS was lower than that of OLA, which may be due to the need for acid dissociation of DAS. In conclusion, the in vitro release results showed that HDO-NPs were pH-sensitive, which was conducive to realize the responsive release of DAS and OLA in the tumor microenvironment.

Cell Uptake and Drug Accumulation

To research the targeting effect of HDO-NPs on tumor cells, HA-DAS nanomicelles labeled with coumarin 6 (C6) were co-cultured with MDA-MB-231 cells for 1 h and 4 h, and the uptake of nanomicelles by cells was observed under the

Table 1 Size, PDI, Zeta Potentia, DL and EE of the HDO-NPs

Size (nm)	PDI	Zeta Potential (mV)	DL/DAS (%)	DL/OLA (%)	EE/OLA (%)
56.18 ± 1.30	0.23 ± 0.02	-7.42 ± 1.22	1.68 ± 0.29	7.38 ± 0.17	84.95 ± 1.17

Notes: The results are expressed as the mean \pm SD, n = 3.

Abbreviations: PDI, polydispersity index; DL, drug loading; EE, encapsulation efficiency; DAS, dasatinib; OLA, olaparib; HDO-NPs, HA-DAS micelle system loaded with OLA.

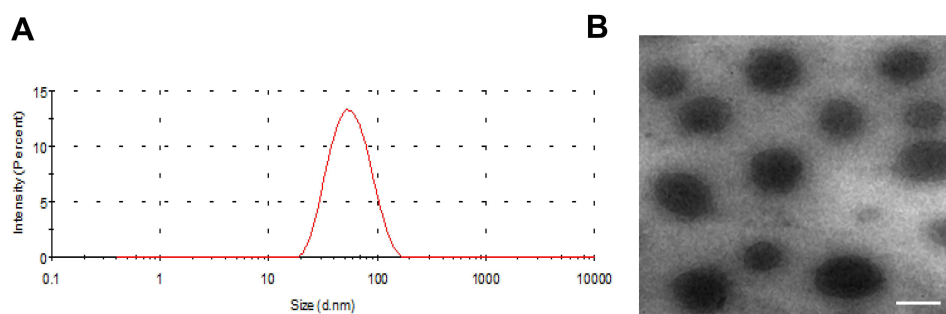


Figure 2 (A) Size distribution of HDO-NPs by DLS. (B) TEM images of HDO-NPs. Scale bar: 50 nm.

Abbreviations: HDO-NPs, HA-DAS micelle system loaded with OLA; DLS, dynamic light scattering; TEM, transmission electron microscopy.

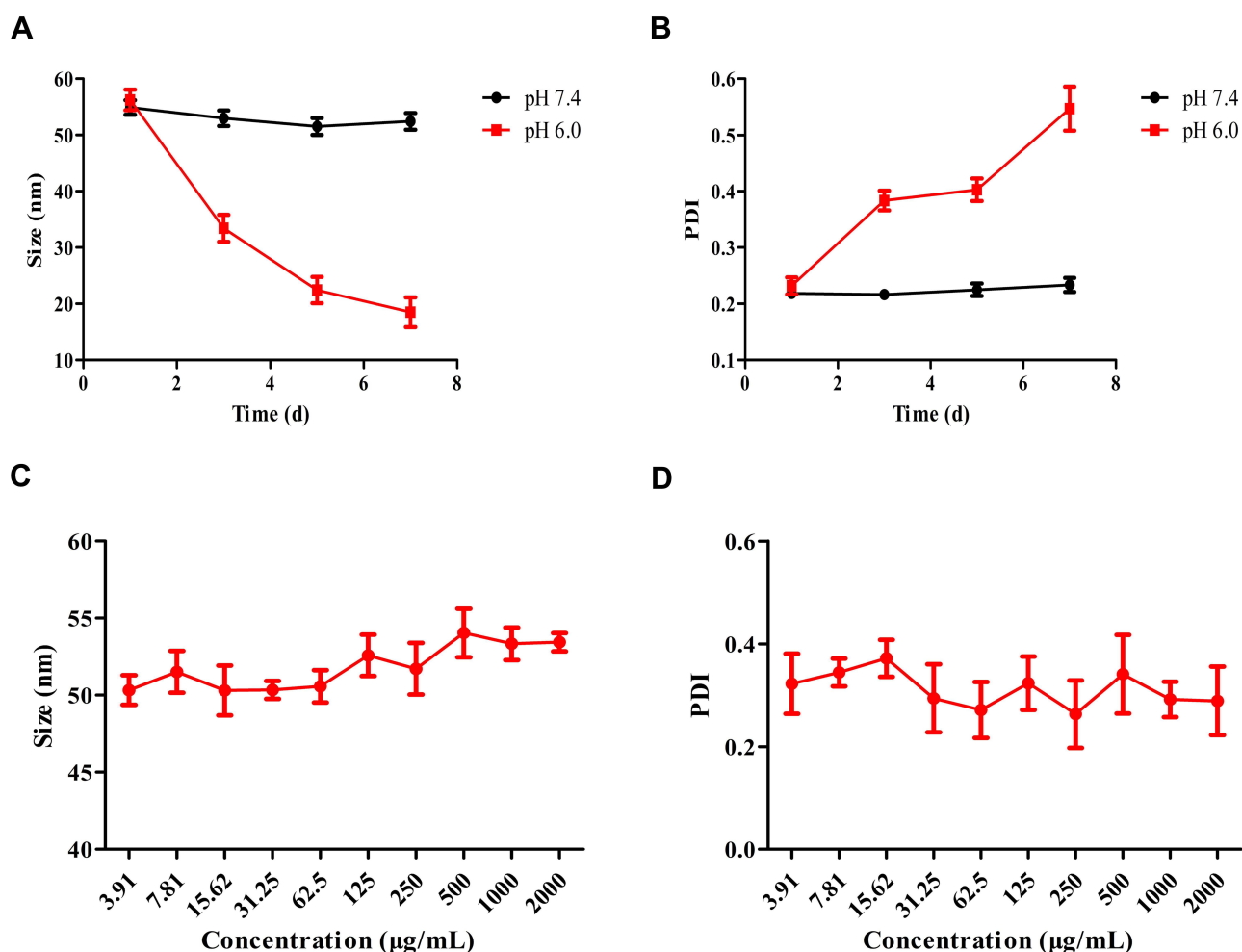


Figure 3 The in vitro stability of HDO-NPs was reflected by (A) size and (B) PDI at pH 6.0 and pH 7.4. The (C) size and (D) PDI at different concentrations were selected to determine the dilution stability of HDO-NPs.

Notes: The results are expressed as the mean \pm SD, $n = 3$.

Abbreviations: HDO-NPs, HA-DAS micelle system loaded with OLA; PDI, polydispersity index.

fluorescence microscope. As shown in Figure 5A and B, owing to the lack of targeting of free C6, weak green fluorescence existed in the cytoplasm. In contrast, a large amount of green fluorescence was observed in the HA-DAS/C6 treatment group, demonstrating that nanomicelles can be effectively absorbed by MDA-MB-231 cells. In addition, blocking the CD44 receptor on the surface of MDA-MB-231 cells with free HA significantly reduced the intracellular fluorescence intensity,

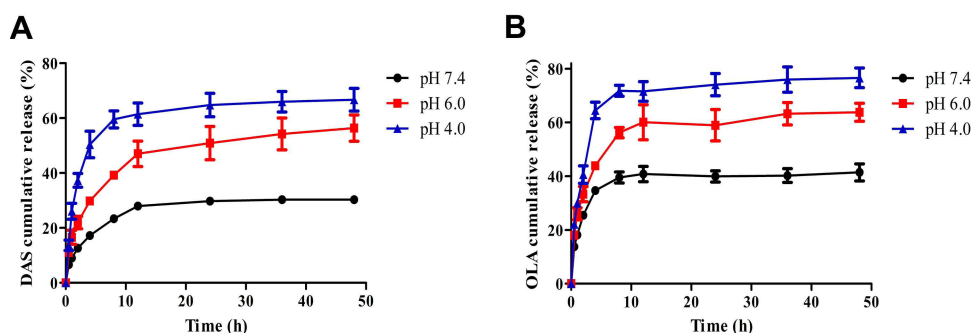


Figure 4 In vitro (A) DAS and (B) OLA release profiles of HDO-NPs at pH 7.4, pH 6.0 and pH 4.0.

Notes: The results are expressed as the mean \pm SD, $n = 3$.

Abbreviations: DAS, dasatinib; OLA, olaparib; HDO-NPs, HA-DAS micelle system loaded with OLA.

due to blockade of the active targeting pathway of nanoparticles.⁴² Therefore, the nanomicelles with HA-DAS as the carrier have better cell targeting. It is worth noting that with the extension of the incubation time, the fluorescence intensity in MDA-MB-231 cells also increased, indicating that the uptake of nanoparticles by cells was time-dependent within 4 h.

The cell uptake experiments showed that HDO-NPs had good cell targeting; however, the effective accumulation of drugs in cells was the key to the efficacy. The accumulative amounts of DAS and OLA in cells at 1, 2 and 4 h were investigated, respectively. As shown in Figure 6A and B, the accumulation of DAS and OLA in the HDO-NPs group was higher than that in the free DAS + OLA group at each time point, owing to the introduction of hyaluronic acid, which could be better taken up by tumor cells and increase drug endocytosis.³⁸ Meanwhile, the drug accumulations in the HA blocking group were lower than that in the HDO-NPs group, which also reflected the above conjecture, further showing that the targeting of HA can enhance the accumulation of drugs in cells.

Intracellular Transport Behavior of HDO-NPs

Micelles enter the cell by endocytosis and then enter the cytoplasm by the intron-lysosome pathway. In this study, the intracellular transport process of micelles was investigated by co-localization of micelles and lysosomes. As shown in Figure 7, the green fluorescence of C6 overlapped with the red fluorescence of lysosomes at 1 h, showing the yellow fluorescence signal, indicating that HDO-NPs were uptaken by tumor cells and transported through the intron-lysosomal pathway.⁴³ After incubation for 4 h, part of the green fluorescence signal was separated from the red signal of lysosomes, illustrating that after micelles entered lysosomes, they dissociated and released C6 in the acidic environment of lysosomes, and then C6 escaped from lysosome and entered the cytoplasm.

Cytotoxicity of HDO-NPs

MTT assays were used to examine the toxicity of OLA, DAS, OLA + DAS and HDO-NPs to MDA-MB-231 cells. The results showed that in Figure 8A and B and Table 2, the OLA group had low toxicity to MDA-MB-231 cells, because free OLA could only act on tumor cells with certain gene deletions. In contrast, the toxicity of other groups was significantly concentration-dependent and time-dependent. It is worth noting that the survival rate of the DAS + OLA group was significantly lower than that of DAS group and OLA group, demonstrating that the two have synergistic effects. In addition, with increasing drug dose and incubation time, the cell survival rate of the HDO-NPs group was markedly lower than that of the DAS + OLA group. The reason was that micelles increased the water solubility and targeting of drugs, increased the concentration of drugs in cells, and showed a stronger inhibitory effect on cells. The IC₅₀ value reflected the same results (Table 3).

To further intuitively respond to the anti-tumor effect of HDO-NPs, the calcein-AM/PI double staining fluorescence method was used to study the anti-tumor activity of nanomicelles. The living cells and dead cells were stained and labeled, to visually analyze the anti-tumor activity of the nanomicelles. As shown in Figure 8C, there was no obvious red appearance in the OLA group, substantiating that free OLA had little toxicity to cells. Moreover, red fluorescence appeared in the other

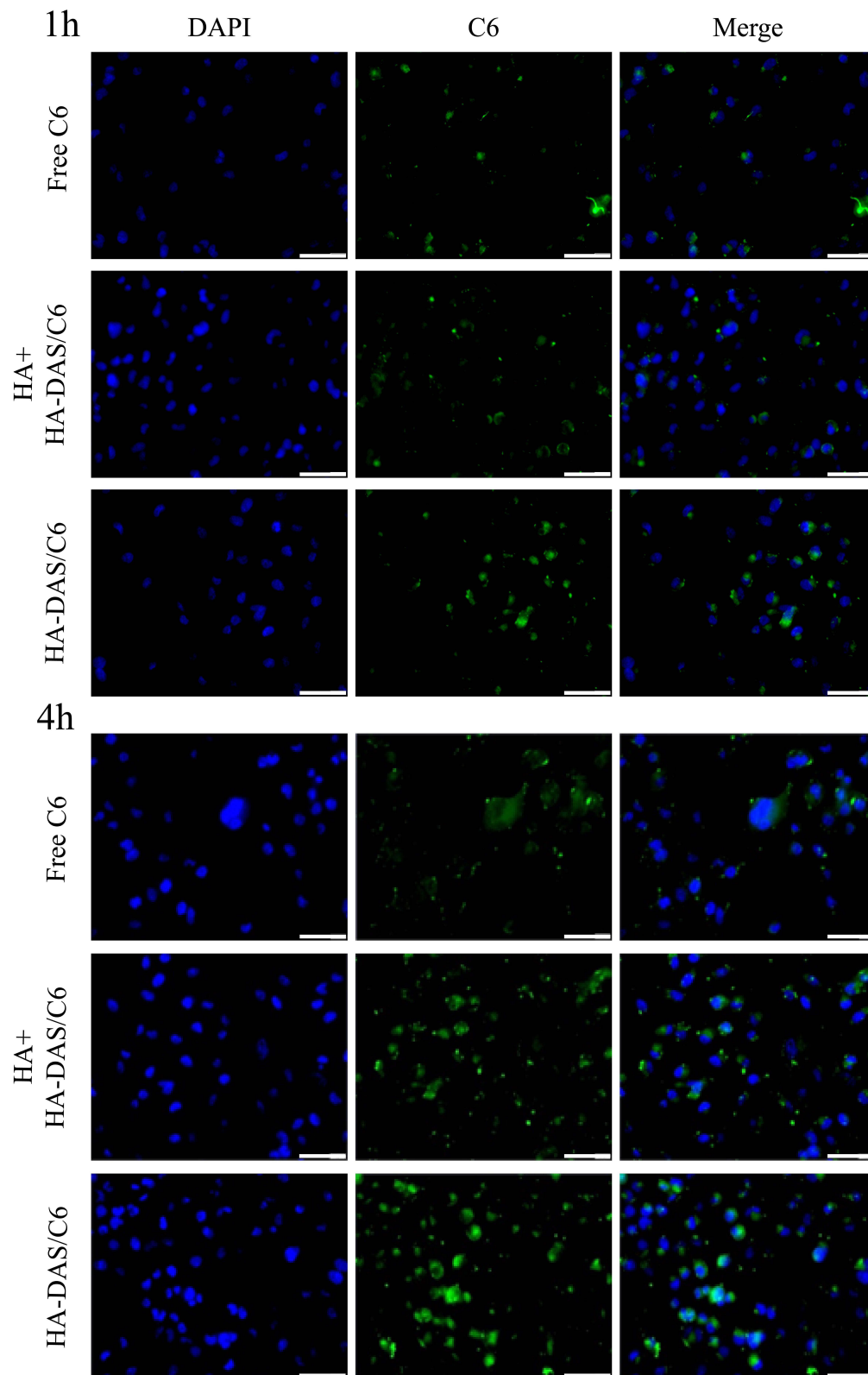


Figure 5 Images of the cellular uptake of C6, HA + HA-DAS/C6 (receptor blocking group) and HA-DAS/C6 against MDA-MB-231 cells at 1 h and 4 h. Scale bar = 50 μ m.
Abbreviations: C6, coumarin 6; HA, hyaluronic acid; HA-DAS/C6, HA-DAS micelle system loaded with C6.

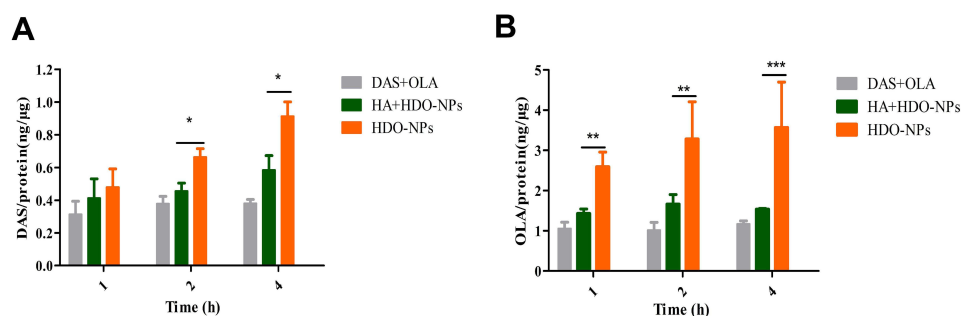


Figure 6 The accumulation of (A) DAS and (B) OLA in MDA-MB-231 cells incubated with DAS + OLA, HA + HDO-NPs and HDO-NPs for different times.

Notes: The results are expressed as the mean \pm SD, $n = 3$; * $p < 0.05$, ** $p < 0.01$ and *** $p < 0.001$.

Abbreviations: DAS, dasatinib; OLA, olaparib; HDO-NPs, HA-DAS micelle system loaded with OLA.

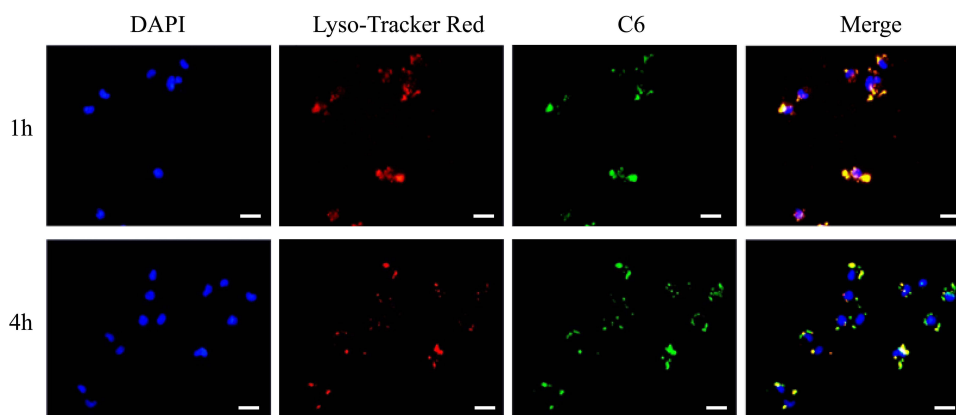


Figure 7 The transport of HDO-NPs in MDA-MB-231 cells. Scale bar = 20 μ m.

Abbreviations: HDO-NPs, HA-DAS micelle system loaded with OLA; C6, coumarin.

drug administration groups, and almost no green fluorescence appeared in the HDO-NPs group, showing that it had the strongest toxicity and good anti-tumor effect, which was consistent with the results of MTT quantitative analysis.

Distribution of HDO-NPs in Mice

Because the *in vivo* treatment was intravenously administered, the effects of HDO-NPs on red blood cells were studied. Even when the concentration of HDO-NPs was 100 μ g/mL, the hemolysis rate was still less than 5%, demonstrating that the prepared polymer micelles had good biocompatibility (Figure 9A and B). Subsequently, the accumulation of HDO-NPs in tumor tissues and their distribution in other organs were detected by MDA-MA-231 tumor-bearing mice model to evaluate the targeting of HA-loaded nanomicelles. Because the free Cy5 was not targeted, it was easily eliminated by the circulatory system, resulting in weak fluorescence intensity in mouse tumor tissues. But the HA-DAS/Cy5 group maintained high fluorescence intensity within 24 h (Figure 9C). After administration for 24 h, the biodistribution of free cy5 and HA-DAS/cy5 in major organs and tumors showed that free Cy5 accumulated less in tumors, while HA-DAS /Cy5 was mainly enriched in tumors (Figure 9D), suggesting that HDO-NPs could effectively accumulate in tumor sites and be used for tumor treatment *in vivo*.

In vivo Anticancer Effects of HDO-NPs

The above experimental results showed that HDO-NPs can be uptaken well by tumor cells, and drug release increases in the microenvironment, which can effectively aggregate in the tumor site. Next, the therapeutic effect of nanoparticles on tumor-bearing mice was investigated, and the treatment process is shown in Figure 10A. We subcutaneously injected tumor cells to establish MDA-MB-231 tumor-bearing mice model. The nude mice were randomly divided into 5 groups

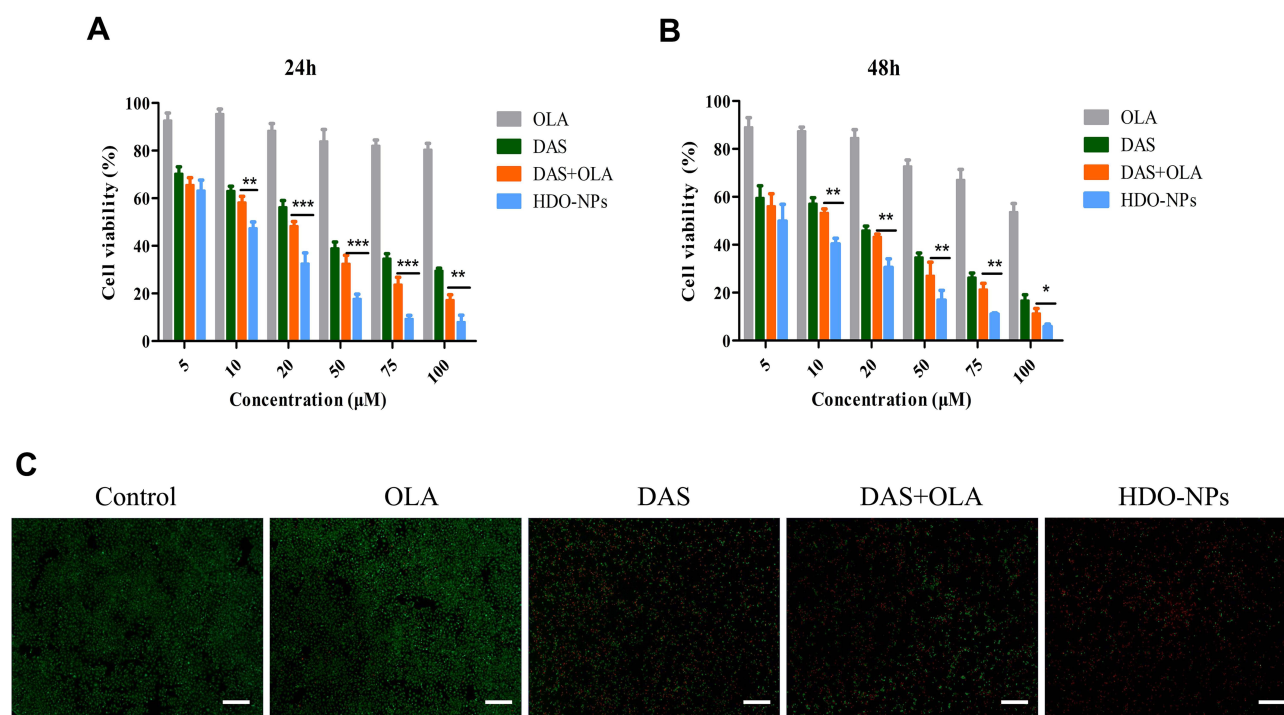


Figure 8 In vitro cytotoxicity analysis of MDA-MB-231 cells after (A) 24 h and (B) 48 h of treatment with free DAS, OLA, DAS + OLA and HDO-NPs. The cell viabilities were determined by MTT cytotoxicity assay. (C) Fluorescent micrographs depicting the cytotoxicity of different drugs. Green represents living cells, and red represents dead cells.

Notes: The results are expressed as the mean \pm SD, $n = 3$, * $p < 0.05$, ** $p < 0.01$ and *** $p < 0.001$. Scale bar = 200 μ m.

Abbreviations: DAS, dasatinib; OLA, olaparib; HDO-NPs, HA-DAS micelle system loaded with OLA.

($n = 6$). The mice were administered once every 3 days 6 times. The body weight and tumor volume were recorded before each administration, and the treatment was completed on the 18th day. As shown in Figure 10B–E, the PBS group had no therapeutic effect, so the tumor grew fastest. In addition, the inhibition of tumor growth in the DAS + OLA treatment group was stronger than that in the free DAS and free OLA treatment groups, suggesting that the two drugs can

Table 2 The Statistical Analysis of Cell Viabilities of MDA-MB-231 Cells Treated with Free DAS, OLA, DAS + OLA and HDO-NPs for 24 h and 48 h

24h						
Groups	p values					
	5μM	10μM	20μM	50μM	75μM	100μM
OLA vs (DAS+OLA)	$p < 0.001$	$p < 0.001$	$p < 0.001$	$p < 0.001$	$p < 0.001$	$p < 0.001$
DAS vs (DAS+OLA)	ns	$p < 0.05$	$p < 0.05$	ns	$p < 0.01$	$p < 0.01$
(DAS+OLA) vs HDO-NPs	ns	$p < 0.01$	$p < 0.001$	$p < 0.001$	$p < 0.001$	$p < 0.01$
48h						
Groups	p values					
	5μM	10μM	20μM	50μM	75μM	100μM
OLA vs (DAS+OLA)	$p < 0.001$	$p < 0.001$	$p < 0.001$	$p < 0.001$	$p < 0.001$	$p < 0.001$
DAS vs (DAS+OLA)	$p < 0.05$	ns	$p < 0.05$	$p < 0.05$	ns	$p < 0.05$
(DAS+OLA) vs HDO-NPs	$p < 0.05$	$p < 0.01$	$p < 0.01$	$p < 0.01$	$p < 0.01$	$p < 0.05$

Notes: "ns" to indicate no significance ($p > 0.05$). " $p < 0.05$, $p < 0.01$, and $p < 0.001$ " means statistical significance.

Abbreviations: DAS, dasatinib; OLA, olaparib; HDO-NPs, HA-DAS micelle system loaded with OLA.

Table 3 In vitro Cytotoxicity of MDA-MB-231 Cells After 24 h and 48 h Incubation with Different Drug Formulations as Determined by MTT Assay

Groups	IC ₅₀ (μM)	
	24 h	48 h
HDO-NPs	12.93 ± 4.68	7.57 ± 1.79
DAS+OLA	20.05 ± 2.14*	15.39 ± 4.83*
DAS	25.04 ± 6.99	19.44 ± 2.51
OLA	NA	246 ± 25.65

Notes: The results are expressed as the mean ± SD, n = 3. *p < 0.05 (HDO-NPs vs DAS + ROZ).

Abbreviations: NA, not available; DAS, dasatinib; OLA, olaparib; HDO-NPs, HA-DAS micelle system loaded with OLA.

also exert synergistic effects in vivo. Compared with the DAS + OLA group, the HDO-NPs group showed significant tumor inhibition, which was related to the improved water-solubility and targeting of the two drugs by micelles. Meanwhile, the tumor growth inhibition rate (TGI) of each group was calculated (Figure 10F). The TGI of HDO-NPs was about 72.31%, which was significantly higher than that of DAS + OLA (56.53%) and DAS (49.83%). On the 18th day of treatment, the weight of mice in each group increased slightly, showing that micelle nanoparticles had good safety (Figure 10G).

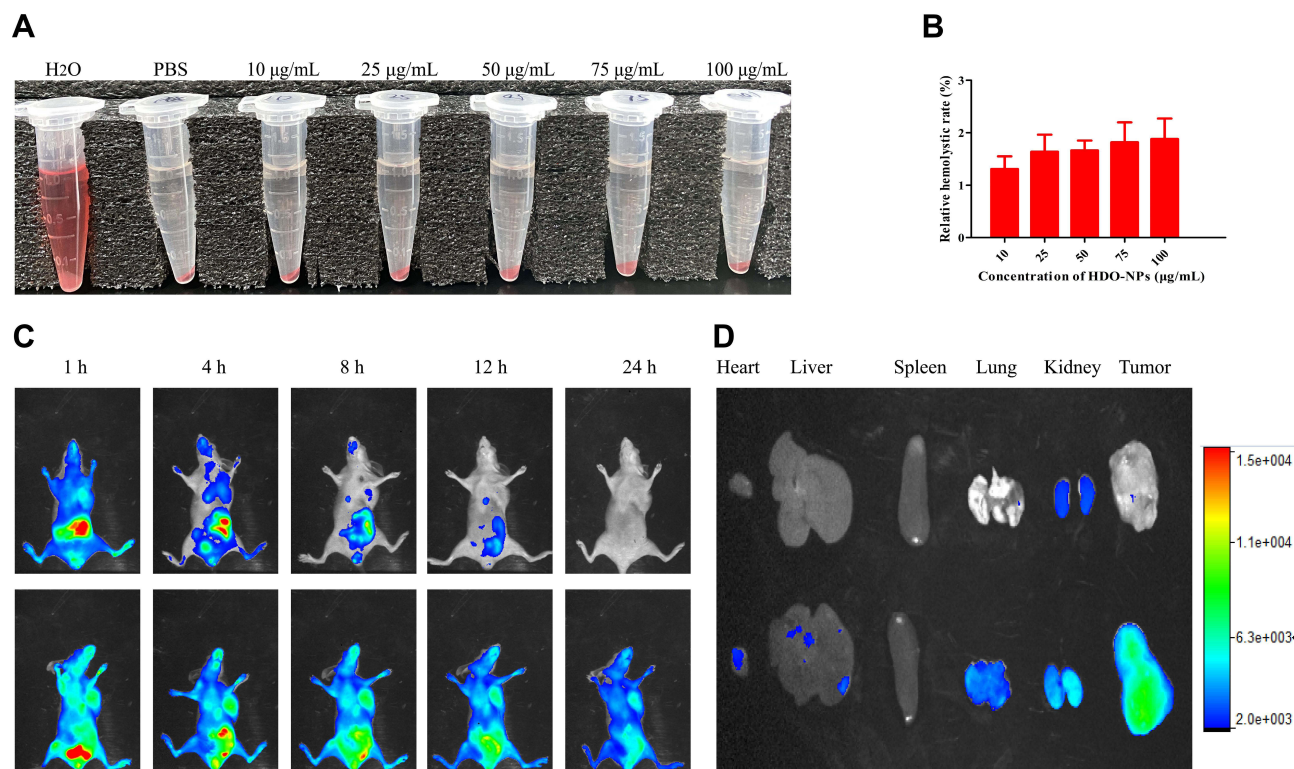


Figure 9 (A) Photographs of the red blood cell hemolysis assay of HDO-NPs with different concentrations, using normal PBS and water as the negative and positive controls. (B) Hemolysis rates of HDO-NPs with different concentrations. In vivo fluorescence imaging of MDA-MB-231 tumors at different time points after intravenous injection (C) and (D) fluorescence imaging of isolated organs and tumor tissues 24 h after intravenous injection (the upper panel shows free Cy5, and the lower panel shows HA-DAS/Cy5).

Notes: The results are expressed as the mean ± SD, n = 3.

Abbreviations: HDO-NPs, HA-DAS micelle system loaded with OLA; Cy5, cyanine 5; HA-DAS/Cy5, HA-DAS micelle system loaded with Cy5.

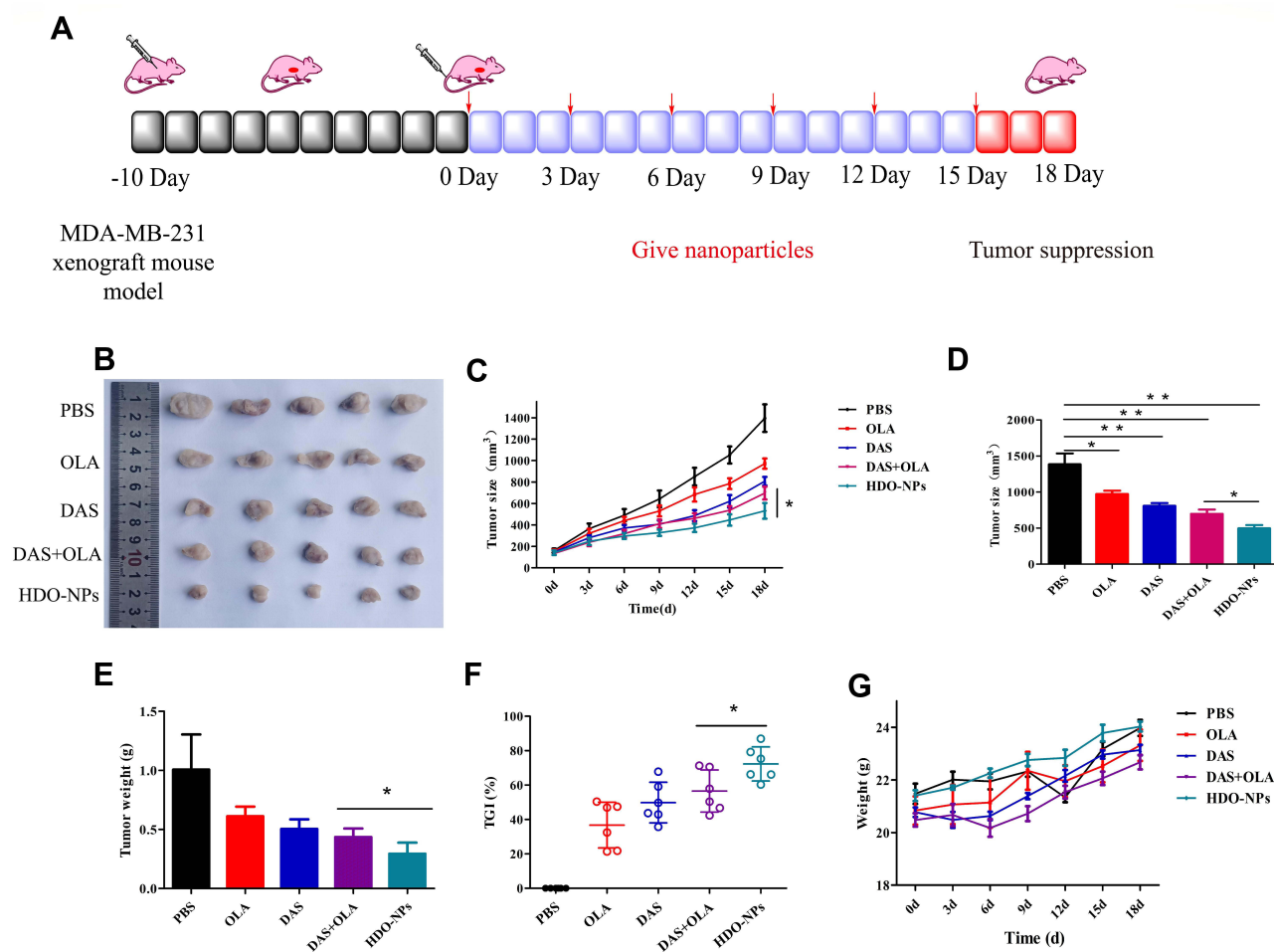


Figure 10 Therapeutic effects in vivo. **(A)** Schematic illustration of the in vivo therapeutic process. Images of isolated tumors **(B)** and tumor volume changes **(C)** of mice in each group during the treatment period. Tumor weight **(D)**, tumor weight **(E)** and TGI **(F)** in each group after the end of treatment. **(G)** The average body weight of mice was used to evaluate the toxicity of the different treatments.

Notes: The results are expressed as the mean \pm SD, $n = 6$, * $p < 0.05$ (DAS + OLA vs HDO-NPs).

Abbreviations: DAS, dasatinib; OLA, olaparib; HDO-NPs, HA-DAS micelle system loaded with OLA; TGI, tumor growth inhibition.

We further studied the potential anti-tumor mechanism of HDO-NPs and analyzed the tumor tissue by HE staining. In the HDO-NPs treatment group, as shown in the red circle in [Figure 11A](#), there was a large area of apoptosis in the tumor tissue. Ki67 was a cell proliferation antigen, indicating the proliferation of cells. The measurement results are shown in [Figure 11B](#). Compared with other groups, the expression signal of Ki67 in the HDO-NPs treatment group was the weakest, suggesting that the proliferation of tumor cells was significantly reduced and that apoptotic cells were increased after treatment. To further explore the underlying mechanism of this synergistic effect, we performed immunofluorescence staining of histone phosphorylation products (γ -H2AX) to evaluate DNA double strand breaks in tumors. As shown in [Figure 11C](#), the expression of γ -H2AX in tumor tissues treated with HDO-NPs was significantly higher than that in other treatment groups, indicating that the treatment group exacerbated the double-strand break of tumor DNA.

In summary, the therapeutic effect of the HDO-NPs treatment group was significantly better than that of the DAS + OLA treatment group of tumors. The result was attributed to the active targeting effect generated by the specific binding of HA and CD44 protein and the passive targeting effect generated by nanoparticles through the EPR effect, to achieve targeted drug delivery and improve drug efficacy.

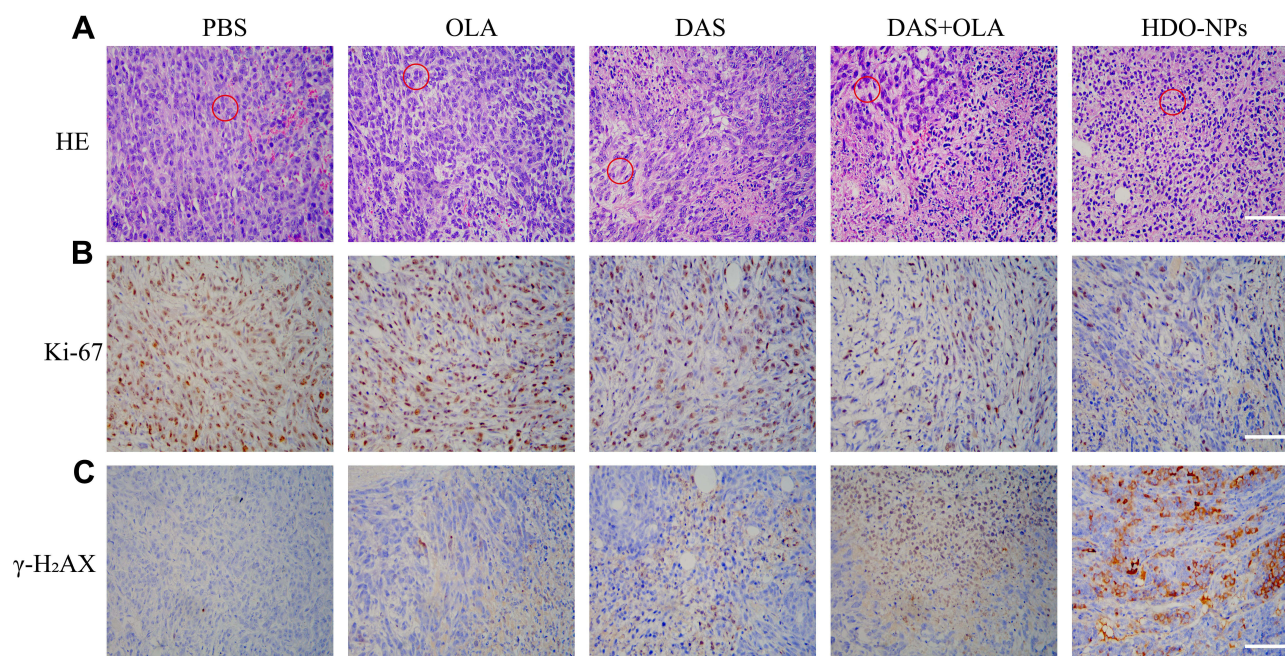


Figure 11 HE staining, Ki-67 staining, and γ -H₂AX staining of tumors after different treatments. Scale bar = 50 μ m. The red circles indicate apoptotic tumor sites.
Abbreviations: DAS, dasatinib; OLA, olaparib; HDO-NPs, HA-DAS micelle system loaded with OLA; HE, hematoxylin eosin.

Biosafety Assessment of HDO-NPs

After treatment, the safety of HDO-NPs was further evaluated. Aspartate aminotransferase (AST) and alanine aminotransferase (ALT) were used to evaluate liver function (Figure 12A and B). Blood urea nitrogen (BUN) and creatinine (CRE) were used to assess renal function (Figure 12C and D). Compared with normal mice, several indicators of the OLA group and DAS + OLA group were significantly increased, suggesting that two free drugs can cause liver and kidney damage. Surprisingly, there was no significant difference between the HDO-NPs group and the normal group, which further confirmed that the nanocarriers we prepared can reduce adverse drug reactions and improve drug safety. Furthermore, the HE staining results of the heart, liver, spleen, lung and kidney in each group (Figure 13) were consistent with the above indicators, and nanoparticles significantly reduced the toxicity of drugs. These results showed that the drug-loaded micelles had good biocompatibility and almost no toxicity to other normal tissues.

In vivo Pharmacokinetic Study

We investigated the pharmacokinetics of nanoparticles via tail vein injection. As shown in Figure 14, free DAS and OLA were quickly cleared from plasma. In contrast, the protective amphiphilic shell greatly extended the circulation time of the two drugs in the blood and increased the half-lives by 1.44-fold (DAS) and 2.46-fold (OLA), respectively. Table 4 shows the pharmacokinetic parameters of the two drugs. As shown in Table 3, the CL value of DAS in HDO-NPs was 0.23-fold that of free DAS, certifying that the clearance rate of DAS in the blood was significantly reduced, which prolonged the circulation time of DAS in vivo and improved the retention efficiency of DAS. Meanwhile, the parameters of MRT, V_{ss}, AUC₀₋₂₄ and AUC_{0-∞} in the HDO-NPs group were 2.71-, 0.643-, 3.75- and 3.22-fold of those in the DAS group, respectively, showing that the drug content in plasma was significantly increased, which improved the bioavailability of DAS. In addition, the changes of OLA pharmacokinetic parameters in the two groups (Table 3) indicated that the inclusion of OLA into nanoparticles could significantly reduce the plasma clearance rate, increase the circulation time in the blood, and improve its bioavailability. It showed that DAS and OLA loaded in HDO-NPs can make the drug be absorbed at a higher concentration and have a stronger systemic effect.

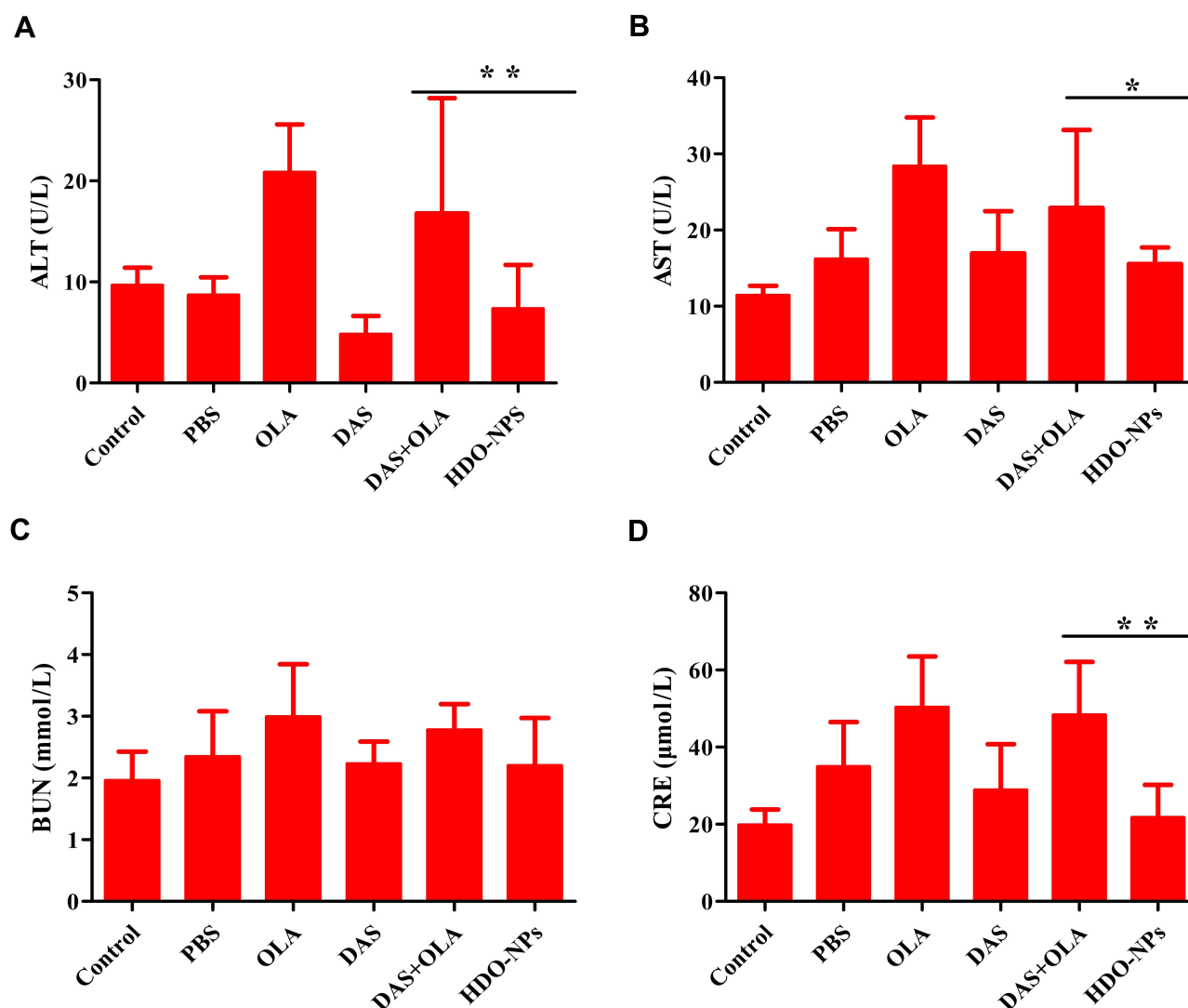


Figure 12 In vivo toxicology examination of mice treated with HDO-NPs. Serum biochemistry data of liver function markers, including (A) alanine aminotransferase (ALT) and (B) aspartate aminotransferase (AST). (C) Blood urea nitrogen (BUN) and (D) creatinine (CRE) of the hematology assay.

Notes: The results are expressed as the mean \pm SD, $n = 3$. * $p < 0.05$, ** $p < 0.01$.

Abbreviations: HDO-NPs, HA-DAS micelle system loaded with OLA; ALT, alanine aminotransferase; AST, aspartate aminotransferase; BUN, blood urea nitrogen; CRE, creatinine.

Conclusion

In this study, we successfully designed polymer prodrug micelles with active HA targeting and pH-sensitive targeting to treat triple negative breast cancer by synergistic DAS and OLA. The hydroxyl group of DAS was linked to the carboxyl group of HA to form an amphiphilic carrier, and the micellar system HDO-NPs with dual targeting nanoparticles was constructed with OLA as the core. On the one hand, HDO-NPs had good stability in vitro and could be effectively released in simulated tumor microenvironment, which can improve the water solubility of DAS and OLA and increase the uptake of nanoparticles by tumor cells. On the other hand, in vitro and in vivo efficacy experiments had proven that micellar particles can effectively increase the therapeutic effect and reduce the adverse reactions of drugs. This study provides an effective strategy for the design of nanomedicines with high selectivity and enhanced antitumor effects for triple negative breast cancer.

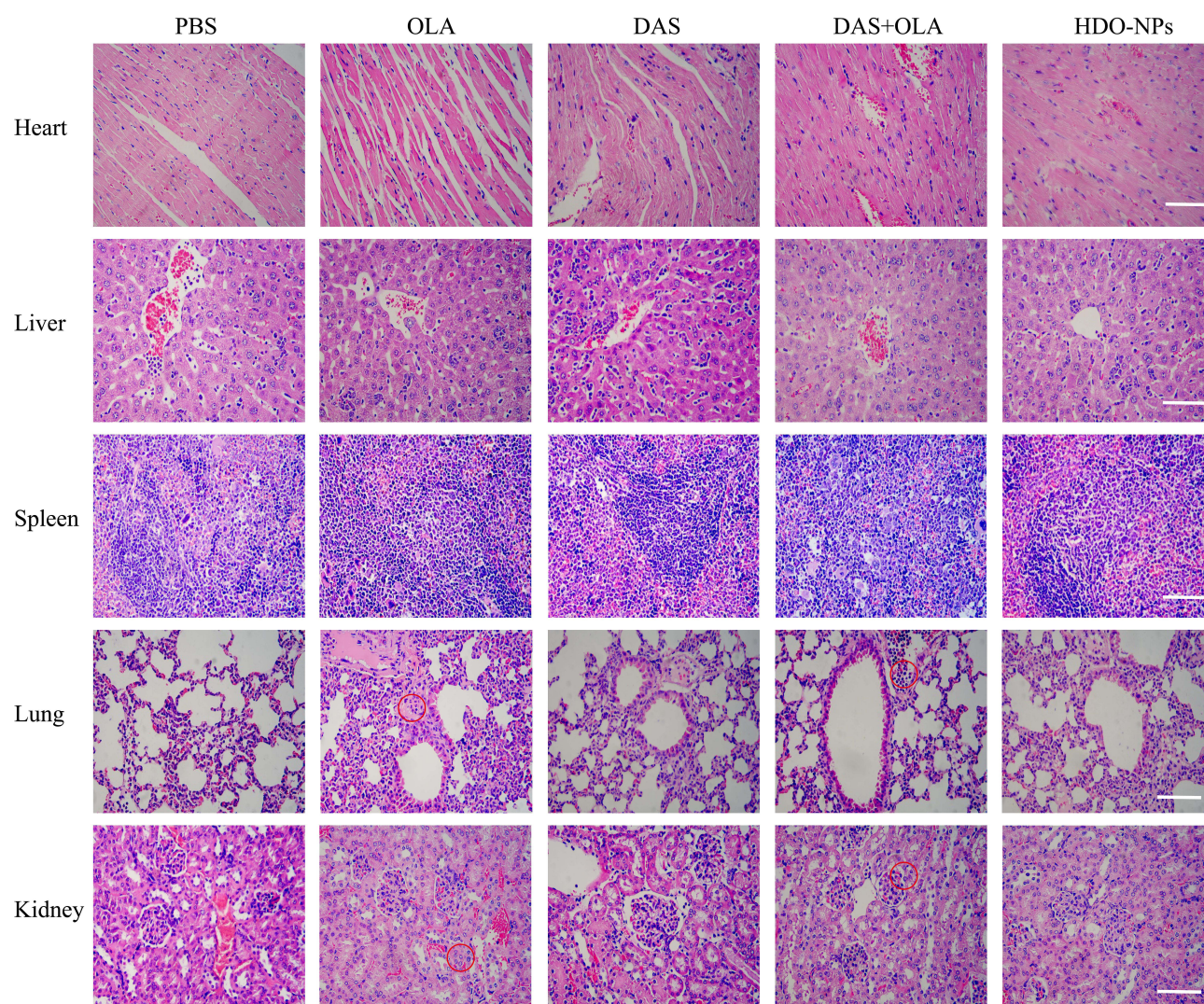


Figure 13 HE staining of various organs in BALB/c nude mice harboring MDA-MB-231 tumor xenografts after different treatments. Scale bar = 200 μ m. The red circles indicate the sites of organ damage.

Abbreviation: HE, hematoxylin eosin.

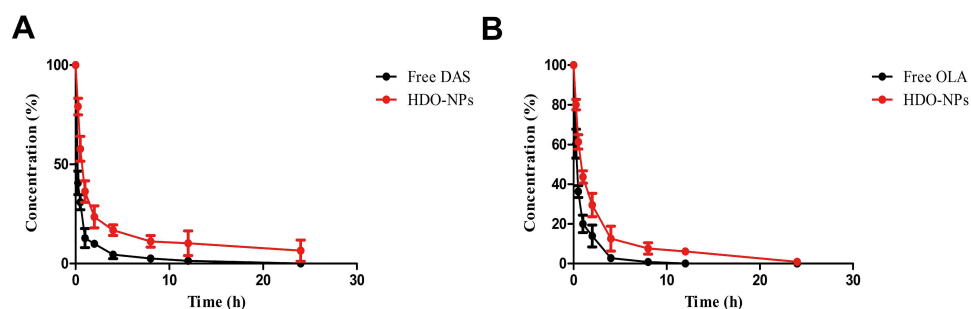


Figure 14 (A) Pharmacokinetics of DAS in free DAS and HDO-NPs. (B) Pharmacokinetics of OLA in free OLA and HDO-NPs.

Notes: The results are expressed as the mean \pm SD, n = 6.

Abbreviations: DAS, dasatinib; OLA, olaparib; HDO-NPs, HA-DAS micelle system loaded with OLA.

Table 4 The Pharmacokinetic Parameters of DAS a) and OLA b) After Injection of HDO-NPs and DAS + OLA

a		
PK Parameters	Groups	
	Free DAS	HDO-NPs
$t_{1/2}$ (h)	3.469 ± 1.758	5.009 ± 0.685*
CL (L/h)	1.260 ± 0.493	0.296 ± 0.069**
MRT (h)	3.780 ± 0.498	10.252 ± 2.426*
V _{ss} (L)	4.604 ± 1.335	2.962 ± 0.587*
AUC ₀₋₂₄ [μg/(mL h)]	2.068 ± 0.751	7.758 ± 1.590**
AUC _{0-∞} [μg/(mL h)]	2.745 ± 2.235	8.834 ± 2.166**
b		
PK Parameters	Groups	
	Free OLA	HDO-NPs
$t_{1/2}$ (h)	1.791 ± 0.594	4.415 ± 1.830^
CL (L/h)	0.133 ± 0.010	0.047 ± 0.012^
MRT (h)	1.517 ± 0.143	6.183 ± 1.813^
V _{ss} (L)	0.201 ± 0.022	0.287 ± 0.083
AUC ₀₋₂₄ [μg/(mL h)]	18.647 ± 1.433	48.144 ± 14.718^^
AUC _{0-∞} [μg/(mL h)]	18.909 ± 1.326	55.353 ± 13.976^^

Notes: The results are expressed as the mean ± SD, n = 6. * $p < 0.05$, ** $p < 0.01$ (DAS in HDO-NPs vs free DAS), ^ $p < 0.05$, ^^ $p < 0.01$ (OLA in HDO-NPs vs free OLA).

Abbreviations: $t_{1/2}$, elimination half-life; CL, clearance rate; MRT, mean residence time; V_{ss}, volume of distribution at steady state; AUC₀₋₂₄, area under the plasma concentration-time curve from time 0 h to 24 h of quantifiable concentration; AUC_{0-∞}, area under the plasma concentration-time curve from time 0 extrapolated to infinite time; DAS, dasatinib; OLA, olaparib; HDO-NPs, HA-DAS micelle system loaded with OLA.

Acknowledgments

The authors would like to thank the Scientific Research Projects of Bengbu Medical College of Anhui Province (No. 2020byzd015), the Key Program of Anhui University Natural Science Research (No. KJ2021A0700) and Scientific Research Innovation Projects of Bengbu Medical College of Anhui Province (No. Byycx21031) for the financial support.

Disclosure

The authors report no conflicts of interest in this work.

References

- Wang J, Zhao H, Zhi K, et al. Exploration of the natural active small-molecule drug-loading process and highly efficient synergistic antitumor efficacy. *ACS Appl Mater Interfaces*. 2020;12(6):6827–6839. doi:10.1021/acsami.9b18443
- Ye M, Han Y, Tang J, et al. A tumor-specific cascade amplification drug release nanoparticle for overcoming multidrug resistance in cancers. *Adv Mater*. 2017;29(38):1702342. doi:10.1002/adma.201702342
- Wang S, Yu G, Wang Z, et al. Enhanced antitumor efficacy by a cascade of reactive oxygen species generation and drug release. *Angew Chem Int Ed Engl*. 2019;58(41):14758–14763. doi:10.1002/anie.201908997
- Hou X, Lin H, Zhou X, et al. Novel dual ROS-sensitive and CD44 receptor targeting nanomicelles based on oligomeric hyaluronic acid for the efficient therapy of atherosclerosis. *Carbohydr Polym*. 2020;232:115787. doi:10.1016/j.carbpol.2019.115787
- Liu Y, Liu Y, Zang J, et al. Design strategies and applications of ROS-responsive phenylborate ester-based nanomedicine. *ACS Biomater Sci Eng*. 2020;6(12):6510–6527. doi:10.1021/acsbiomaterials.0c01190
- He Y, Lei L, Cao J, et al. A combinational chemo-immune therapy using an enzyme-sensitive nanoplatfor for dual-drug delivery to specific sites by cascade targeting. *Sci Adv*. 2021;7(6). doi:10.1126/sciadv.aba0776.
- Zhang M, Qin X, Zhao Z, et al. A self-amplifying nanodrug to manipulate the Janus-faced nature of ferroptosis for tumor therapy. *Nanoscale Horiz*. 2022;7(2):198–210. doi:10.1039/D1NH00506E

8. Li Q, Zhou Y, He W, et al. Platelet-armored nanoplatfrom to harmonize janus-faced IFN-gamma against tumor recurrence and metastasis. *J Control Release*. 2021;338:33–45. doi:10.1016/j.jconrel.2021.08.020
9. Zhou S, Shang Q, Wang N, et al. Rational design of a minimalist nanoplatfrom to maximize immunotherapeutic efficacy: four birds with one stone. *J Control Release*. 2020;328:617–630. doi:10.1016/j.jconrel.2020.09.035
10. Zhang M, Qin X, Xu W, et al. Engineering of a dual-modal phototherapeutic nanoplatfrom for single NIR laser-triggered tumor therapy. *J Colloid Interface Sci*. 2021;594:493–501. doi:10.1016/j.jcis.2021.03.050
11. Wang P, Gong Q, Hu J, et al. Reactive Oxygen Species (ROS)-responsive prodrugs, probes, and theranostic prodrugs: applications in the ROS-related diseases. *J Med Chem*. 2021;64(1):298–325. doi:10.1021/acs.jmedchem.0c01704
12. Xu L, Zhao M, Zhang H, et al. Cinnamaldehyde-based poly(ester-thioacetal) to generate reactive oxygen species for fabricating reactive oxygen species-responsive nanoparticles. *Biomacromolecules*. 2018;19(12):4658–4667. doi:10.1021/acs.biomac.8b01423
13. Chang N, Zhao Y, Ge N, et al. A pH/ROS cascade-responsive and self-accelerating drug release nanosystem for the targeted treatment of multi-drug-resistant colon cancer. *Drug Deliv*. 2020;27(1):1073–1086. doi:10.1080/10717544.2020.1797238
14. Sun B, Luo C, Yu H, et al. Disulfide bond-driven oxidation- and reduction-responsive prodrug nanoassemblies for cancer therapy. *Nano Lett*. 2018;18(6):3643–3650. doi:10.1021/acs.nanolett.8b00737
15. Liu G, Lovell JF, Zhang L, et al. Stimulus-responsive nanomedicines for disease diagnosis and treatment. *Int J Mol Sci*. 2020;21(17):6380.
16. Dai L, Li X, Duan X, et al. A pH/ROS cascade-responsive charge-reversal nanosystem with self-amplified drug release for synergistic oxidation-chemotherapy. *Adv Sci*. 2019;6(4):1801807. doi:10.1002/advs.201801807
17. Chen Y, Yao Y, Zhou X, et al. Cascade-reaction-based nanodrug for combined chemo/starvation/chemodynamic therapy against multidrug-resistant tumors. *ACS Appl Mater Interfaces*. 2019;11(49):46112–46123. doi:10.1021/acsami.9b15848
18. Liu J, Liu W, Weitzhandler I, et al. Ring-opening polymerization of prodrugs: a versatile approach to prepare well-defined drug-loaded nanoparticles. *Angew Chem Int Ed Engl*. 2015;54(3):1002–1006. doi:10.1002/anie.201409293
19. Lu B, Xiao Z, Wang Z, et al. Redox-sensitive polymer micelles based on CD44 and folic acid receptor for intracellular drug delivery and drug controlled release in cancer therapy. *ACS Appl Bio Mater*. 2019;2(10):4222–4232. doi:10.1021/acsabm.9b00500
20. Choi KY, Han HS, Lee ES, et al. Hyaluronic acid-based activatable nanomaterials for stimuli-responsive imaging and therapeutics: beyond CD44-mediated drug delivery. *Adv Mater*. 2019;31(34):e1803549. doi:10.1002/adma.201803549
21. Xu X, Zeng Z, Huang Z, et al. Near-infrared light-triggered degradable hyaluronic acid hydrogel for on-demand drug release and combined chemo-photodynamic therapy. *Carbohydr Polym*. 2020;229:115394. doi:10.1016/j.carbpol.2019.115394
22. Lu B, Xiao F, Wang Z, et al. Redox-sensitive hyaluronic acid polymer prodrug nanoparticles for enhancing intracellular drug self-delivery and targeted cancer therapy. *ACS Biomater Sci Eng*. 2020;6(7):4106–4115. doi:10.1021/acsbiomaterials.0c00762
23. Lv Y, Xu C, Zhao X, et al. Nanoplatfrom assembled from a CD44-targeted prodrug and smart liposomes for dual targeting of tumor microenvironment and cancer cells. *ACS Nano*. 2018;12(2):1519–1536. doi:10.1021/acsnano.7b08051
24. Liu J, Huang Y, Kumar A, et al. pH-sensitive nano-systems for drug delivery in cancer therapy. *Biotechnol Adv*. 2014;32(4):693–710. doi:10.1016/j.biotechadv.2013.11.009
25. Kankala RK, Liu CG, Chen AZ, et al. Overcoming multidrug resistance through the synergistic effects of hierarchical pH-sensitive, ROS-generating nanoreactors. *ACS Biomater Sci Eng*. 2017;3(10):2431–2442. doi:10.1021/acsbiomaterials.7b00569
26. Cao Z, Wang X, Pang Y, et al. Biointerfacial self-assembly generates lipid membrane coated bacteria for enhanced oral delivery and treatment. *Nat Commun*. 2019;10(1):5783. doi:10.1038/s41467-019-13727-9
27. Lan S, Liu Y, Shi K, et al. Acetal-functionalized pillar[5]arene: a pH-responsive and versatile nanomaterial for the delivery of chemotherapeutic agents. *ACS Appl Bio Mater*. 2020;3(4):2325–2333. doi:10.1021/acsabm.0c00086
28. Xue X, Jin S, Zhang C, et al. Probe-inspired nano-prodrug with dual-color fluorogenic property reveals spatiotemporal drug release in living cells. *ACS Nano*. 2015;9(3):2729–2739. doi:10.1021/nn5065452
29. Lui G, Shaw R, Schaub FX, et al. BET, SRC, and BCL2 family inhibitors are synergistic drug combinations with PARP inhibitors in ovarian cancer. *EBioMedicine*. 2020;60:102988. doi:10.1016/j.ebiom.2020.102988
30. Zeng F, Ju RJ, Liu L, et al. Efficacy in treating lung metastasis of invasive breast cancer with functional vincristine plus dasatinib liposomes. *Pharmacology*. 2018;101(1–2):43–53. doi:10.1159/000480737
31. Yao Q, Choi JH, Dai Z, et al. Improving tumor specificity and anticancer activity of dasatinib by dual-targeted polymeric micelles. *ACS Appl Mater Interfaces*. 2017;9(42):36642–36654. doi:10.1021/acsami.7b12233
32. Robson M, Im SA, Senkus E, et al. Olaparib for metastatic breast cancer in patients with a germline BRCA mutation. *N Engl J Med*. 2017;377(6):523–533. doi:10.1056/NEJMoal706450
33. Kaufman B, Shapira-Frommer R, Schmutzler RK, et al. Olaparib monotherapy in patients with advanced cancer and a germline BRCA1/2 mutation. *J Clin Oncol*. 2015;33(3):244–250. doi:10.1200/JCO.2014.56.2728
34. Chakraborty G, Patail NK, Hirani R, et al. Attenuation of SRC kinase activity augments PARP inhibitor-mediated synthetic lethality in BRCA2-altered prostate tumors. *Clin Cancer Res*. 2021;27(6):1792–1806. doi:10.1158/1078-0432.CCR-20-2483
35. Corrales-Sanchez V, Noblejas-Lopez M, Nieto-Jimenez C, et al. Pharmacological screening and transcriptomic functional analyses identify a synergistic interaction between dasatinib and olaparib in triple-negative breast cancer. *J Cell Mol Med*. 2020;24(5):3117–3127. doi:10.1111/jcmm.14980
36. Leveque D, Becker G, Bilger K, et al. Clinical pharmacokinetics and pharmacodynamics of dasatinib. *Clin Pharmacokinet*. 2020;59(7):849–856. doi:10.1007/s40262-020-00872-4
37. Wang H, Zhang Y, Zeng X, et al. A combined self-assembled drug delivery for effective anti-breast cancer therapy. *Int J Nanomedicine*. 2021;16:2373–2388. doi:10.2147/IJN.S299681
38. Zhang Y, Zeng X, Wang H, et al. Dasatinib self-assembled nanoparticles decorated with hyaluronic acid for targeted treatment of tumors to overcome multidrug resistance. *Drug Deliv*. 2021;28(1):670–679. doi:10.1080/10717544.2021.1905751
39. Fan Y, Wang Q, Lin G, et al. Combination of using prodrug-modified cationic liposome nanocomplexes and a potentiating strategy via targeted co-delivery of gemcitabine and docetaxel for CD44-overexpressed triple negative breast cancer therapy. *Acta Biomater*. 2017;62:257–272. doi:10.1016/j.actbio.2017.08.034

40. Sykes EA, Chen J, Zheng G, et al. Investigating the impact of nanoparticle size on active and passive tumor targeting efficiency. *ACS Nano*. 2014;8(6):5696–5706. doi:10.1021/nn500299p
41. Wang Y, Wang F, Liu Y, et al. Glutathione dectonated and pH responsive nano-clusters of Au nanorods with a high dose of DOX for treatment of multidrug resistant cancer. *Acta Biomater*. 2018;75:334–345. doi:10.1016/j.actbio.2018.06.012
42. Zhong Y, Goltzsche K, Cheng L, et al. Hyaluronic acid-shelled acid-activatable paclitaxel prodrug micelles effectively target and treat CD44-overexpressing human breast tumor xenografts in vivo. *Biomaterials*. 2016;84:250–261. doi:10.1016/j.biomaterials.2016.01.049
43. Zhu J, Huo Q, Xu M, et al. Bortezomib-catechol conjugated prodrug micelles: combining bone targeting and aryl boronate-based pH-responsive drug release for cancer bone-metastasis therapy. *Nanoscale*. 2018;10(38):18387–18397. doi:10.1039/C8NR03899F

International Journal of Nanomedicine

Dovepress

Publish your work in this journal

The International Journal of Nanomedicine is an international, peer-reviewed journal focusing on the application of nanotechnology in diagnostics, therapeutics, and drug delivery systems throughout the biomedical field. This journal is indexed on PubMed Central, MedLine, CAS, SciSearch®, Current Contents®/Clinical Medicine, Journal Citation Reports/Science Edition, EMBase, Scopus and the Elsevier Bibliographic databases. The manuscript management system is completely online and includes a very quick and fair peer-review system, which is all easy to use. Visit <http://www.dovepress.com/testimonials.php> to read real quotes from published authors.

Submit your manuscript here: <https://www.dovepress.com/international-journal-of-nanomedicine-journal>